# Experimental study of the performance and emission characteristics of an adapted commercial four-cylinder spark ignition engine running on hydrogen-methane mixtures

P.M. Diéguez, J.C. Urroz, S. Marcelino-Sádaba, A. Pérez-Ezcurdia, M. Benito-Amurrio, D. Sáinz, L.M. Gandía*

*Escuela Técnica Superior de Ingenieros Industriales y de Telecomunicación, Universidad Pública de Navarra, Campus de Arrosadía, E-31006 Pamplona, Spain*

* Corresponding author. Phone: +34 948 169 605. Fax: +34 948 169 606.

*E-mail addresses:* pmde@unavarra.es (P.M. Diéguez); lgandia@unavarra.es (L.M. Gandía).

**Abstract**

The use of hydrogen/methane mixtures with low methane contents as fuels for internal combustion engines (ICEs) may help to speed up the development of the hydrogen energy market and contribute to the decarbonization of the transportation sector. In this work, a commercial 1.4 l four-cylinder Volkswagen spark-ignition engine previously adapted to operate on pure hydrogen has been fueled with hydrogen/methane mixtures with 5-20 vol. % methane (29.6-66.7 wt. %). An experimental program has been executed by varying the fuel composition, air-to-fuel ratio ($\lambda$), spark advance and engine speed. A discussion of the results regarding the engine performance (brake torque, brake mean effective pressure, thermal efficiency) and emissions (nitrogen oxides, CO and unburned hydrocarbons) is presented. The results reveal that $\lambda$ is the most influential variable on the engine behavior due to its marked effect on the combustion temperature. As far as relatively high values of $\lambda$ have to be used to

prevent knock, the effect on the engine performance is negative. In contrast, the specific emissions of nitrogen oxides decrease due to a reduced formation of thermal $NO_x$. A clear positive effect of reducing the spark advance on the specific $NO_x$ emissions has been observed as well. As concerns CO and unburned hydrocarbons (HCs), their specific emissions increase with the methane content of the fuel mixture, as expected. However, they also increase as $\lambda$ increases in spite of the lower fuel concentration due to a proportionally higher reduction of the power. Finally, the effect of the increase of the engine speed is positive on the CO and HCs emissions but negative on that of $NO_x$ due to improved mixing and higher temperature associated to intensified turbulence in the cylinders.

*Keywords: Adapted SI engine; Hydrogen-methane mixtures; Hydrogen energy; Internal combustion engine; Emissions; Transportation sector.*

**Nomenclature**

| | |
|---|---|
| BTDC | before top dead center |
| BMEP | brake mean effective pressure |
| $c_p$ | specific heat, J/(mol·K) |
| CNG | compressed natural gas |
| $C_{NO_x}$ | $NO_x$ concentration in the engine exhaust, ppm |
| CO | carbon monoxide |
| EGR | exhaust gas recirculation |
| $h_f^0$ | specific enthalpy of formation at the standard state, J/mol |
| $\Delta h$ | specific enthalpy change, J/mol |
| HCs | unburned hydrocarbons |

| | |
|---|---|
| HHV | higher heating value |
| $H_2ICE$ | hydrogen-fueled ICE |
| ICE | internal combustion engine |
| MBP | maximum brake power (kW) |
| MBT | maximum brake torque (N·m) |
| $M_{NO_x}$ | $NO_x$ molecular weight, g/mol |
| $\dot{n}$ | molar flow rate, mol/s |
| $N_e$ | exhaust moles formed per mol of fuel |
| NGVs | natural gas-fueled vehicles |
| $NO_x$ | nitrogen oxides |
| $[NO_x]$ | specific $NO_x$ emissions, g/kW·h |
| $P$ | engine effective power, kW |
| $\dot{Q}$ | power associated to the heat losses, W |
| $R$ | universal gas constant, 8.314 J/(mol·K) |
| $SA$ | spark advance (º BTDC) |
| SI | spark-ignition |
| $T$ | temperatura, K or ºC |
| $\dot{V}_f$ | fuel flow rate, normal l/min |
| $\dot{W}$ | power delivered by the engine, W |

*Subscripts*

| | |
|---|---|
| $e$ | exit |
| $f$ | formation |

| | |
|---|---|
| *i* | inlet |
| *P* | products |
| *ref* | reference |
| *R* | reactants |

*Greek letters*

| | |
|---|---|
| $\alpha$ | independent term for $c_p/R$ in Eq. 4 |
| $\eta$ | molar fraction of methane in the fuel mixture |
| $\lambda$ | air-to-fuel ratio |

## 1. Introduction

One of the most likely uses of hydrogen energy in the future is in the transportation sector. Whereas fuel cells, batteries and electric engines offer efficient solutions for the propulsion of vehicles, internal combustion engines (ICEs) have potential to speed up the development of a hydrogen energy market due to their availability, versatility, reliability and relatively low cost. The lack of a distribution and delivery infrastructure and the very high economic cost of introducing one are recognized as key obstacles for the widespread use of hydrogen in the short term [1]. In contrast, natural gas has a well-established distribution network. Moreover, compressed natural gas (CNG) has been used for long time as fuel for ICEs, particularly spark-ignition (SI) engines in natural gas-fueled vehicles (NGVs) [2].

Natural gas has very good fuel properties mainly due to its high octane number (120-130) that allows for increased compression ratios without risk of detonation resulting in thermal efficiencies comparable to that of gasoline-fueled ICEs. On the other hand, methane is characterized by lower volumetric efficiency but higher air-to-fuel ratio ($\lambda$) at stoichiometric conditions compared with gasoline [3]. The result of these factors is that the power output of a natural gas-fueled engine is typically 10-15 % below that of a gasoline engine [4]. Of course, strategies such as direct-injection [5], turbocharching [6] and intercooling can improve the power output although operation under these conditions often leads to increased nitrogen oxides ($NO_x$) emissions [4]. Exhaust gas recirculation (EGR) is frequently used for reducing $NO_x$ emissions from ICEs but in the case of natural gas-fueled engines, the cycle-by-cycle variations of the cylinder peak pressure and the maximum rate of pressure rise increase with the EGR ratio [7]. Nevertheless, fuel-lean operation is required to limit $NO_x$ emissions. In this regard, methane shows some drawbacks associated to its relatively low flame propagation velocity that under lean-burn operation can lead to incomplete combustion, increased cycle-by-cycle variations and occasional flame failure [8]. Adding hydrogen to natural gas extends the lean limit of combustion; in this way, extremely low emissions can be achieved. More specifically, Sierens and Rosseel [9] showed that the best strategy is to adjust the fuel composition (hydrogen content) as a function of the engine load without throttling. So, at low loads, pure hydrogen could be used at high air-to-fuel ratios ($\lambda > 2$). At intermediate loads, a low-hydrogen mixture (*e.g.* hythane: 20 vol. % hydrogen, 80 vol. % methane) can be employed to maintain $NO_x$ emissions at low level ($\lambda > 1.5$) but using exhaust aftertreatment for CO and unburned hydrocarbons. At full load nearly pure methane would have to be used for achieving high brake mean effective pressure. On the other hand, the very high flame speed of hydrogen allows shorter combustion duration, and leads to higher peak and total cycle heat fluxes and a smaller lag between ignition and heat flux peak compared with methane, as found by Demuynck et al. [10]. Moreover, hydrogen addition has a pronounced effect on reducing the cyclic variability of the indicated mean effective pressure [11]. From a complementary point of view, adding methane to hydrogen allows extending the rich-fuel operating region while reducing the risk of hydrogen combustion anomalies such as backfire and knock [12,13].

From the above discussion it is clear that hydrogen/natural gas mixtures have great interest as fuel for ICEs. As a matter of fact, there is a considerable literature on the subject. Several authors have reviewed the works published till the 1997-2003 period [3,9,14,15]; more recent papers by Kahraman et al. [16], Akansu and Bayrak [17] and Mariani et al. [18] include an update of the state-of-the-art. Very recently, Klell et al. [19] have performed a very interesting and thorough update of the advantages, synergies, potential and regulatory aspects of the use of hydrogen/methane mixtures in ICEs. Much of the published studies mainly deal with investigating how the addition of relatively low hydrogen amounts (below 30 vol. %) to natural gas/methane increases the thermal efficiency and improves the engine performance; great attention is also paid to the emissions [20,21]. In these studies, the influence of some individual variables such as $\lambda$, the injection timing and EGR ratio is investigated [5,7,15-18,22-25]. As natural gas is a fossil energy source, an increasing number of papers is appearing on the use of hydrogen/biogas mixtures. Used biogas comes from the anaerobic digestion of biomass or organic wastes [26-28], or is a model gas produced by mixing pure methane and carbon dioxide [29]. The use of gases obtained from the catalytic decomposition of biogas has been also reported [30]. In much of the published works, the results on the use of hydrogen/methane mixtures were obtained on single-cylinder dedicated ICEs which are very versatile research tools [31]. There are also studies with bigger commercial engines. Sierens and Rosseel [9] employed a Crusader T7400 eight-cylinder in V SI engine with a displacement volume of 7.4 l and compression ratio of 8.5:1. The engine, based on the GM 454 one, was adapted for use of gaseous fuels. Ma et al. [6,24,32] used an in-line six-cylinder Dongfeng Motor Co. Ltd. engine originally designed for city bus application. The CNG turbocharged SI engine had a displacement volume of 6.2 l and operated with a compression ratio of 10.5:1. Wang et al. [33] worked with an in-line six-cylinder Weifang diesel engine converted to run on CNG with a compression ratio of 16:1. Park et al. [34] used a heavy-duty turbocharged six-cylinder natural gas-fueled Doosan Infracore Inc. engine with a displacement volume of 11 l. Akansu and coworkers [15-17] carried out a series of studies with a four-cylinder 1.8 l SI Ford engine. Song and coworkers [28,29] employed a turbocharged gas engine generator with a four-cylinder SI engine fueled with biogas/hydrogen mixtures. Thurnheer et al. [22] used a 2 l four-cylinder engine with a compression ratio of 13.5:1 and Wang et al. [35] a three-cylinder engine. Genovese et al. [36] reported on road experimental tests with buses equipped with Mercedes turbocharged six-cylinder engines of 6.9 l and 170 kW that were fed with fuel mixtures containing 5-25 vol. % hydrogen. Klell et al. [19] have developed a flex-fuel prototype vehicle capable of operating with any mixture of natural gas and hydrogen based on a 1.8 l four-cylinder supercharged engine. Mariani et al. [18] have recently reported on the performance of a Fiat Panda 1.2 NP equipped with a four-cylinder SI engine of 38 kW at 5000 rpm operated with a compression ratio of 9.8:1 and fuelled with mixtures containing 15 and 30 vol.% hydrogen. Park et al. [37] used a heavy duty 11 l six-cylinder engine of a city bus.

In previous papers by our group we have reported on the modifications carried out to adapt the gasoline SI engine of a Volkswagen Polo 1.4 to be fueled with hydrogen [38]. A gasoline carbureted engine-generator set was also converted to an electronic fuel-injected power unit capable to operate bi-fuel (hydrogen-gasoline) [39]. Later on, a commercial Volkswagen Polo 1.4 A04 vehicle was adapted to run bi-fuel, that is, with gasoline or hydrogen as desired by the driver [40]. In the present work we have investigated the performance of the four-cylinder Volkswagen engine adapted to run on hydrogen [38] fed with hydrogen/methane mixtures. A collection of experimental data has been obtained by varying the hydrogen content of the fuel mixture, $\lambda$ and the engine load and speed. This work has been carried out in the framework of a project devoted to the production and applications of renewable hydrogen obtained from water electrolysis and wind energy [41-44].

Main novelty of this work lies on the fact that, in contrast with most the previously published papers, fuel mixtures with relatively low methane contents, up to 20 vol. %, are considered. It should be noted that this apparently low content is in reality much higher when it is expressed as mass percentage (up to 66.7 wt. % methane) so we decided to restrict the study to this composition. While there is considerable information available on the performance of ICEs running on methane-rich mixtures, say above 70 vol. % methane (94.9 wt. %), which is an interesting use of hydrogen for improving the combustion characteristics of methane and accelerating the introduction of hydrogen in the energy system, there exists much less information on the performance of these engines running on fuels more convenient for contributing to the decarbonization of the transportation sector. So, using low-methane content mixtures has really the potential of reducing the environmental impact, provided that hydrogen is obtained from renewable sources. These mixtures are also interesting because pure hydrogen should be used at high values of $\lambda$ in naturally aspirated port fuel injection spark ignition ICEs to prevent combustion anomalies such as pre-ignition and backfiring. Adding methane to hydrogen extends the rich-fuel limit of hydrogen combustion thus allowing engine operation with fuel-air mixtures closer to stoichiometric conditions due to the good knock resistant properties of methane resulting in higher brake torque and power [45]. Of course, direct-injection or turbocharging of pure hydrogen can be used to improve the power output but these solutions require a much more complex and expensive adaptation of our original ICE that is outside the scope of this study.

## 2. Engine and experimental equipment and methods

The Volkswagen engine and test bed cell used in this study were described in detail in a previous paper [38]. It is an in-line four-cylinder naturally aspirated port fuel injection spark ignition engine with a displacement volume and compression ratio of 1.4 l and 10.5:1, respectively. Running on gasoline, the engine provided maximum brake torque (MBT) and maximum brake power (MBP) of 132 N·m at 3800 rpm and 59 kW at 5000 rpm, respectively. The engine was adapted to run on hydrogen ($H_2$ICE) modifying the fuel feeding and electronic management systems. The gasoline injectors were substituted by hydrogen injectors (Quantum Technologies), and a metallic gas accumulator was manufactured and connected to the injectors to maintain constant the pressure at the injectors' inlet. The original electronic control unit was replaced by a programmable MoTeC M400 unit. The original lambda sensor was replaced by a wideband lambda sensor (Bosch LSU 4.9) suitable for lean operation. The modified engine was tested in a bed cell consisting of an eddy current dynamometer AVL 80 that provided precisions for torque and engine speed of ± 0.2 % and ± 1 rpm, respectively. Running on pure hydrogen, it provided a MBT of 63 N·m at 3800 rpm and MBP of 32 kW at 5000 rpm. These modest values were in part due to the conservative operation conditions adopted retarding the ignition advance to values far from producing knock. The brake thermal efficiency of the $H_2$ICE was greater than that of the gasoline engine except for $\lambda > 1.8$. A significant effect of the spark advance on the $NO_x$ emissions was found; operation at $\lambda$ ratios higher than 1.8 produced low $NO_x$ emissions of the order of 50-75 ppm.

Sensors and actuators were connected to the MoTeC M400 unit and calibrated. Flow meters (Bronkhorst) provided the hydrogen and air mass flow rates with a precision of ± 0.5 %. Pressure and temperature in the intake manifold were recorded with a Bosch 03C.906.051 apparatus. The crankshaft angle and pressure in cylinder number 1 were measured by using a Kistler 6117BFD47 sensor with precisions of ± 0.02 º and ± 0.6 %, respectively. A Bosch ETT 008.31 analyzer was attached to determine CO (± 0.001 %), $CO_2$

(± 0.1 %) and unburned hydrocarbons (HCs, ± 2 ppm) in the exhaust gases. A Horiba MEXA-720NOx analyzer was used to determine $NO_x$ (precision of ± 2 ppm). There was no catalyst mounted on the exhaust.

In this work, pure hydrogen and hydrogen/methane mixtures with volumetric methane content of 5, 10 and 20 % have been considered. The mixtures were prepared and delivered by Air Liquide in gas cylinders of 50 l at 200 bar hat were mounted in the experimental test bed cell described in a previous work [38]. The fuel feeding line includes two pressure reduction stages. The first one consists of a high-pressure regulator connected to the gas cylinders that reduces the pressure to 9 bar. In the second stage the pressure is further reduced to 3 bar means of a pressure regulator that gives access to a gas accumulator connected to the fuel injectors.

The flammability limits have critically conditioned the design of the experiments. As it is well-known, hydrogen has a very wide flammability range but combustion anomalies such as backfire and knock prevent for using low air-to-fuel ratios. For this reason, values of $\lambda$ above 1.6 were typically used. The usual experimental procedure was to set the engine speed and change the throttle opening thus allowing the test bed cell to provide a resistance torque. Several engine speeds between 2000 and 5000 rpm were employed for each set of experimental conditions. Runs were typically conducted at full load. Optimum injection timing and spark advance maps were first obtained for maximum engine power or efficiency. As these maps were almost coincident, the criterion of maximum thermal efficiency was finally adopted.

## 3. Results and discussion

In what follows the results of the engine performance and emission characteristics will be presented and discussed. Due to the strong influence of the combustion temperature on the engine performance and on the combustion process and other chemical reactions leading to the formation of pollutants such as $NO_x$, it is illustrative starting with an analysis of the maximum (adiabatic) flame temperature and its dependence on two relevant operating variables for this study: the fuel composition and $\lambda$.

Application of the first law of thermodynamics to the combustion process leads to

$$\dot{Q} + \dot{W} = \sum_{e=1}^{P} \dot{n}_e \left( h_f^0 + \Delta h \right)_e - \sum_{i=1}^{R} \dot{n}_i \left( h_f^0 + \Delta h \right)_i \tag{1}$$

where $\dot{Q}$ corresponds to the heat losses, $\dot{W}$ is the power delivered by the engine, $\dot{n}_e$ and $\dot{n}_i$ the molar flow rates of the combustion products ($P$) and reactants ($R$), respectively, $h_f^0$ is the standard specific enthalpy of formation and $\Delta h$ the specific enthalpy change of the exit ($e$) and inlet ($i$) states with respect to the conditions of the standard state (1 atm and 298.15 K). As we are interested in comparing the maximum temperatures, we set $\dot{Q} = 0$ and $\dot{W} = 0$, so the combustion gases result from the cylinder at the so-called adiabatic flame temperature. In such a case Eq. (1) becomes

$$\sum_{e=1}^{P} \dot{n}_e \left( h_f^0 + \Delta h \right)_e = \sum_{i=1}^{R} \dot{n}_i \left( h_f^0 + \Delta h \right)_i \tag{2}$$

Now we will consider the combustion of 1 mol of fuel composed of $\eta$ moles of $CH_4$ and $(1-\eta)$ moles of $H_2$. Assuming complete combustion of the fuel in air with a given air-to-fuel ratio ($\lambda$)

$$\eta CH_4 + (1-\eta) H_2 + \frac{\lambda}{2}(1+3\eta)\left( O_2 + \frac{79}{21} N_2 \right) \rightarrow$$

$$\eta CO_2 + (1+\eta) H_2O + \frac{\lambda - 1}{2}(1+3\eta) O_2 + \frac{\lambda}{2}(1+3\eta)\frac{79}{21} N_2 \tag{3}$$

Combining Eqs. 2 and 3 assuming that $\Delta h$ can be taken as 0 for the reactants because they are at conditions close to the standard state, and that all the compounds are ideal gases with specific heat $c_p$ given by

$$c_p/R = \alpha + \beta T + \gamma T^2 + ... \tag{4}$$

where $T$ is the temperature and $R$ the universal gas constant, and that $\Delta h$ can be approximated by

$$\Delta h = \alpha R\left(T - T_{ref}\right) \tag{5}$$

where $T_{ref}$ is a reference temperature, the adiabatic flame temperature becomes

$$T = T_{ref} + \frac{\eta h^0_{f\,CH_4} - [\eta h^0_{f\,CO_2} + (1+\eta)h^0_{f\,H_2O}]}{R\left[\eta \alpha_{CO_2} + (1+\eta)\alpha_{H_2O} + \frac{\lambda - 1}{2}(1+3\eta)\alpha_{O_2} + \frac{\lambda}{2}\frac{79}{21}(1+3\eta)\alpha_{N_2}\right]} \tag{6}$$

Fig. 1 shows the evolution of the adiabatic flame temperature as a function of the fuel composition and the air-to-fuel ratio obtained solving Eq. 6 taking $T_{ref}$ = 25 ºC and the values of $h^0_f$ and $\alpha$ found in [46]. As can be seen, the adiabatic flame temperature strongly depends on $\lambda$ and decreases as the air-to-fuel ratio increases due to the lower fuel content of the mixture and the diluting effect of the oxygen and nitrogen in excess introduced with the air. As for the fuel composition, the adiabatic flame temperature decreases as the molar or volumetric fraction of methane increases, particularly at low methane contents. Although the higher heating value (HHV) of methane on a molar basis (888 kJ/mol) is about three times higher than that of hydrogen (283.6 kJ/mol), this is more than compensated by the fact that the combustion of 1 mol of methane requires four times more oxygen (or air) than 1 mol of hydrogen.

In practice, combustion temperatures will be obviously lower than the values in Fig. 1 mainly due to the power delivered by the engine and the heat losses. On the other hand, the temperature and pressure in the cylinder strongly depend on the ignition advance. As mentioned in Section 2, in this work, optimum spark advance maps for maximum thermal efficiency were established and adopted.

*3.1. Engine performance*

The brake torque is obviously linked to the power cycle of the gases in the cylinder which in turn depends on the engine speed, load, spark advance and fuel nature. Regarding the hydrogen-methane mixtures, as a representative example of our results, Fig. 2 shows the brake torque as a function of $\lambda$ and the fuel composition at full load, 3400 rpm and optimum spark advance. It can be seen that the brake torque slightly changes with the fuel composition but it clearly decreases as the air-to-fuel ratio increases. This behavior can be interpreted in terms of the effect of the combustion temperature as it is very similar to the evolution of the adiabatic flame temperature, as illustrated in Fig. 1. It is well-known that hydrogen combustion presents the risks of backfire and knock that prevent from operating at low values of $\lambda$. On the other hand, there is no problem on combusting methane at stoichiometric conditions ($\lambda = 1$). Therefore, from the point of view of the engine performance, the addition of methane to hydrogen has the positive effect of allowing fuel richer operation thus increasing the engine torque. As concerns the brake mean effective pressure (BMEP), its values at the conditions of the results shown in Fig. 3 essentially depend on the air-to-fuel ratio. As expected, the BMEP decreases as $\lambda$ increases; in this case from 4.7 bar for $\lambda = 1.6$, to 3.5 bar for $\lambda = 2.0$ and finally, about 2.3 bar for $\lambda = 2.5$.

Fig. 3 shows the results corresponding to the thermal efficiency, that is, the ratio between the effective power and the fuel heating power. Tests were conducted at full load, optimum spark advance and 4200 rpm; similar results were obtained at other engine speeds. It can be seen that the efficiency drops from 34-35 % for $\lambda$ values of 1.6-2.0 to 28-30 % when the air-to-fuel ratio increases up to 2.5. The results show a trend towards lower efficiencies as the methane content of the fuel increases. As for the engine torque, the influence of the operating conditions on the mechanical efficiency can be explained in terms of the influence of the combustion temperature. Indeed, as explained before, the combustion temperature decreases as the methane content of the fuel increases. As a result, the highest efficiencies are obtained when using pure hydrogen. Similarly, the combustion temperature decreases as the fuel mixture becomes leaner (see Fig. 1) thus explaining the decrease of the mechanical efficiency as $\lambda$ increases.

### *3.2. Emission characteristics*

#### *3.2.1. Nitrogen oxides ($NO_x$)*

In this work, the specific $NO_x$ emissions ($[NO_x]$, g/kW·h) have been calculated from the concentration of nitrogen oxides ($C_{NO_x}$ in ppm) measured in the engine exhaust according to the following expression

$$[NO_x] = \frac{60 \cdot 10^{-6}}{22.4} \cdot \frac{\dot{V}_f \cdot N_e \cdot M_{NO_x} \cdot C_{NO_x}}{P} \qquad (7)$$

where $\dot{V}_f$ (normal l/min) is the fuel flow rate, $N_e$ the exhaust moles formed from 1 mol of fuel assuming complete combustion (which depends on $\eta$ and $\lambda$, see Eq. 3), $P$ (kW) the brake power and $M_{NO_x}$ (g/mol) the $NO_x$ molecular weight that has been taken as 30 assuming that the produced nitrogen oxides are mainly formed by NO [47].

As it is well-known, the rate of the chemical reactions producing nitrogen oxides according to the extended Zeldovitch model is favored by the increase of the temperature and the concentration of the reactants ($N_2$ and $O_2$). Obviously, fuel-rich mixtures (low values of

$\lambda$) will favor $NO_x$ formation due to the dominating effect of temperature [18,47-49]. Nevertheless, it is possible through the control of the spark advance (*SA*) to modify the pressure, and then the combustion temperature, reached in the cylinders. The effect of the ignition timing on lean combustion limit when using hydrogen/natural gas as fuel has been by Wang et al. [50]. In our case, the results included in Table 1 correspond to the operation of the modified engine with pure hydrogen at $\lambda$ of 1.6 and 2000 rpm. As can be seen, as the spark advance increases maintaining constant the fuel flow rate, both the maximum pressure and $NO_x$ concentration increase whereas the effective power remains virtually unchanged. Reducing the spark advance from 20 to 10º BTDC (before top dead center) leads to a decrease of the $NO_x$ concentration in the exhaust from 214 to 113 ppm. Fig. 4 shows the experimental pressure-volume diagrams corresponding to the thermodynamic cycles developed under the operating conditions of Table 1. These results are in accordance with those of Park et al. [51] who found that peak cylinder pressures increased with advancing spark timing and increasing the fuel hydrogen content. The heat release rate diagram corresponding to the thermodynamic cycle developed under the operating conditions included in Table 1 at spark advance of 10 º BTDC is shown in Fig. 5. As can be seen the ignition takes place at the end of the compression stroke, at crank angle of 350 º in accordance with the spark advance used in this case. Maximum rate of heat release is reached early during the power stroke at 375 º. After that, the heat release rate starts to decrease with the fuel burning being completed at crank angle of approximately 415 º.

Regarding the influence of the fuel composition, Fig. 6 shows the evolution of the specific $NO_x$ emissions as a function of the spark advance and molar fraction of methane ($\eta$) in the fuel mixture at full load, $\lambda$ of 1.6 and 3400 rpm. As explained above, the specific $NO_x$ emissions increase with the spark advance, however, they strongly decrease with the methane content due to the decrease of the combustion temperature. This is a positive effect of adding methane to hydrogen fuel. When expressed as volumetric concentrations, the values at spark advance of 10º BTDC decrease from 93 ppm for pure hydrogen to 62 ppm for a mixture with $\eta$ = 0.20. However, due to the lower flame speed of methane compared with hydrogen, the spark advance for optimum engine efficiency increases with the methane content compensating for this effect. In fact, as shown in Fig. 7, the specific emissions at optimal spark advance become almost only governed by the air-to-fuel ratio being relatively unaffected by the fuel composition at a given value of $\lambda$ within the limits considered in this study. Only the fuel mixture with the highest methane content ($\eta$ = 0.20) could be combusted under stoichiometric conditions ($\lambda$ = 1). The rest of the fuels, including pure hydrogen, presented tendency to knock that prevented from using values of $\lambda$ lower than 1.6. $NO_x$ emissions under stoichiometric conditions were very high, reaching up to 3.05 g/kW·h in spite of the very low oxygen availability. When using $\lambda$ = 1.6 the emissions were close to 1 g/kW·h and dropped to 0.3-0.4 g/kW·h when the air-to-fuel increased to 2-2.5.

As concerns the influence of the engine speed, it has been found (results not shown) that the specific $NO_x$ emissions increase with the engine speed. For example, at $\lambda$ = 2, full load, $\eta$ = 0.2 and optimum spark advance, the emissions increase from 0.32 to 0.39 and finally 0.47 g/kW·h when the engine speed increases from 3400 to 4200 and finally 5000 rpm. As the engine speed increases the turbulence becomes intensified leading to improved mixing, higher combustion temperatures and $NO_x$ emissions. Nevertheless, the influence of the engine speed on the nitrogen oxides emissions is much less marked than that of the air-to-fuel ratio or the spark advance.

### *3.2.2. Carbon monoxide (CO)*

The influence of the spark advance and fuel composition on the CO emissions at $\lambda$ = 1.6 is shown in Fig. 8 where the solid lines correspond to data obtained at an engine speed of

4200 rpm whereas dash-dotted lines correspond to a lower speed of 3400 rpm. Obviously, the main effect is that of the fuel composition because as the carbon (methane) content of the fuel increases that of CO in the engine exhaust increases as well. It can be seen in Fig. 8 that the emissions increase from virtually 0 with pure hydrogen to about 0.3, 0.45 and 0.8 g/kW·h for fuel mixtures containing 5, 10 and 20 vol. % of methane, respectively. On the other hand, the influence of the spark advance and the engine speed on the emissions of this pollutant is negligible.

As concerns the air-to-fuel ratio, Fig. 9 shows the results obtained at full load, optimum spark advance and engine speed of 3400 rpm. It can be seen that the CO emissions strongly increase with $\lambda$. For example for $\eta$ = 0.10 (10 vol. % methane) the CO emissions at $\lambda$ = 2.5 (3.6 g/kW·h) are almost 7 times higher than when $\lambda$ = 1.6 (0.5 g/kW·h). A possible explanation of this somewhat unexpected result is that, in spite of the lower carbon content of the air/fuel mixture as $\lambda$ increases, a proportionally greater reduction of the power is produced thus leading to increased specific emissions. This reasoning is in accordance with Moreno et al. [45], who found a similar trend regarding the specific $CO_2$ emissions of a naturally aspirated two-cylinder SI engine fueled with hydrogen and methane blends at full load.

Specific CO emissions for $\eta$ = 0.20 under stoichiometric conditions and at $\lambda$ = 2 are almost coincident (about 2.2 g/kW·h) and 3 times higher than at $\lambda$ = 1.6 (about 0.8 g/kW·h). This suggests that stoichiometric conditions neither are favorable for minimum carbon monoxide emissions, probably in this case due to a lack of oxygen availability. For this reason, considerably lower CO emissions are produced at the intermediate $\lambda$ value of 1.6 compared with $\lambda$ = 1 or 2.

*3.2.3. Unburned hydrocarbons (HCs)*

The influence of the spark advance, fuel composition and engine speed on the specific HCs emissions at $\lambda$ = 1.6 is shown in Fig. 10. In this Figure, solid, dotted, dash-dotted and dashed lines correspond to engine speeds of 4200, 3400, 2600 and 1800 rpm, respectively. In principle, it can be assumed that the HCs emissions correspond to unburned methane, so, as expected, the specific emissions increase with the methane content of the fuel, although the emissions are low compared to that of CO. Whereas the emissions of the fuels with $\eta$ = 0.05 and 0.10 are similar, about 0.02 and 0.025 g/kW·h, respectively, they increase significantly for $\eta$ = 0.20. Moreover, for this fuel composition the influence of the engine speed on the HCs emissions becomes apparent. Indeed, the emissions increase from about 0.035 g/kW·h at 4200 rpm to 0.06-0.07 g/kW·h at 1800 rpm. The positive effect of the engine speed reducing the HCs emissions can be explained as the result of improved fuel combustion due to the increased turbulence in the cylinders that should favor the mixing of the reactants. The influence of the spark advance on the HCs emissions is very slight; although a tendency can be appreciated towards increased hydrocarbons emissions as the spark advance decreases.

Regarding the air-to-fuel ratio, Fig. 11 shows the results obtained at full load and optimum spark advance. As in the case of the CO emissions (see Fig. 9), the specific HCs emissions strongly increase with $\lambda$ and as the engine speed decreases. As discussed above for CO, these results can be interpreted in terms of a proportionally greater reduction of the engine power as $\lambda$ increases leading to increased specific emissions. However, in this case, the unburned hydrocarbons monotonously decrease as the air-to-fuel increases. Indeed, for $\eta$ = 0.20 and engine speed of 4200 rpm (solid lines in Fig. 11) the HCs emissions decrease from 0.085 g/kW·h at $\lambda$ = 2.0 to 0.03 g/kW·h at $\lambda$ = 1.6 and 0.02 g/kW·h at stoichiometric conditions.

## 4. Conclusions

An experimental study has been carried out feeding with hydrogen/methane mixtures a commercial 1.4 l Volkswagen four-cylinder spark-ignition engine previously adapted to run on pure hydrogen. In contrast with most of the studies reported in the literature, special attention has been paid to fuel mixtures with low methane content (5-20 vol. %, 29.6-66.7 wt. %). The main motivation of adding relatively small amounts of methane to hydrogen is to extend the rich-fuel limit of hydrogen combustion thus allowing operating at air-to-fuel ratios ($\lambda$) closer to stoichiometric conditions with a reduced risk of combustion anomalies.

It has been found that $\lambda$ is the most influential operating variable on the engine performance due to its marked effect on the combustion temperature. As far as $\lambda$ has to be maintained relatively high to prevent combustion anomalies, mainly knock, but also backfire, the result is a negative effect on parameters such as the engine thermal efficiency and torque due to the lower combustion temperature. Replacing hydrogen by methane up to 20 vol. % does not improve this situation due to the increased amount of air required in a molar basis to combust methane compared to hydrogen.

From the point of view of the specific nitrogen oxides ($NO_x$) emissions, using hydrogen/methane mixtures has positive effects because the decrease of the combustion temperature as both $\lambda$ and the methane content increase leads to lower thermal $NO_x$ formation. Moreover, the emissions can be additionally reduced using suitably low values of the spark advance although the combustion characteristics of methane prevent from using excessively low values of this parameter.

Regarding the CO and hydrocarbons (HCs) specific emissions, there is an obvious negative effect of the presence of methane in the fuel mixture. The specific CO emissions are similar to that of $NO_x$ but an order of magnitude higher than that of HCs. In contrast with the case of the nitrogen oxides, increasing $\lambda$ has negative effects on both CO and HCs specific emissions that can be attributed to a proportionally higher reduction of the power than that of the CO and HCs production. On the other hand, increasing the engine speed reduces the emissions of these pollutants due to the improved mixing associated to the intensified turbulence in the engine cylinders.

**Acknowledgements**

We gratefully acknowledge Acciona Biocombustibles S.A. for its financial support under R&D contract to the Public University of Navarra OTRI 2006 13 118 (CENIT project: SPHERA) and Volkswagen Navarra S.A. for the Volkswagen Polo 1.4 engine donation. LMG and PMD also acknowledge financial support by Ministry of Science and Innovation of the Spanish Government (ENE2012-37431-C03-03).

## References


[1] Rand DAJ, Dell RM. Hydrogen Energy. Challeneges and Prospects. Cambridge, UK: RSC Publishing; 2008. p. 6.

[2] Das LM, Gulati R, Gupta PK. A comparative evaluation of the performance characteristics of a spark ignition engine using hydrogen and compressed natural gas as alternative fuels. Int J Hydrogen Energy 2000; 25: 783-93.

[3] Bauer CG, Forest TW. Effect of hydrogen addition on the performance of methane-fueled vehicles. Part I: effect on S.I. engine performance. Int J Hydrogen Energy 2001; 26: 55-70.

[4] Korakianitis T, Namasivayam AM, Crookes RJ. Natural-gas fueled spark-ignition (SI) and compression-ignition (CI) engine performance and emissions. Prog Energy Combust Sci 2011; 37: 89-112.

[5] Huang Z, Wang J, Liu B, Zeng K, Yu J, Jiang D. Combustion characteristics of a direct-injection engine fueled with natural gas-hydrogen blends under different ignition timings. Fuel 2007; 86: 381-7.

[6] Ma F, Wang M, Jiang L, Chen R, Deng J, Naeve N, Zhao S. Performance and emission characteristics of a turbocharged CNG engine fuelled by hydrogen-enriched compressed natural gas with high hydrogen ratio. Int J Hydrogen Energy 2010; 35: 6438-47.

[7] Huang B, Hu E, Huang Z, Zheng J, Liu B, Jiang D. Cycle-by-cycle variations in a spark ignition engine fuelled with natural gas-hydrogen blends combined with EGR. Int J Hydrogen Energy 2009; 34: 8405-14.

[8] Bade Shrestha SO, Karim GA. Hydrogen as an additive to methane for spark ignition engine applications. Int J Hydrogen Energy 1999; 24: 577-86.

[9] Sierens R, Rosseel E. Variable composition hydrogen/natural gas mixtures for increased engine efficiency and decreased emissions. J Eng Gas Turbines Power 2000; 122: 135-40.

[10] Demuynck J, Raes N, Zuliani M, De Paepe M, Sierens R, Verhelst S. Local heat flux measurements in a hydrogen and methane spark ignition engine with a thermopile sensor. Int J Hydrogen Energy 2009; 34: 9857-68.

[11] Sen AK, Wang J, Huang Z. Investigating the effect of hydrogen addition on cyclic variability in a natural gas spark ignition engine: Wavelet multiresolution analysis. Appl Energy 2011; 88: 4860-6.

[12] Verhelst S, Wallner T. Hydrogen-fueled internal combustion engines. Prog Energy Combust Sci 2009; 35: 490-527.

[13] Verhelst S, Wallner T, Eichlseder H, Naganuma K, Gerbig F, Boyer B, Tanno S. Electricity powering combustion: hydrogen engines. Proc IEEE 2012; 100: 427-39.

[14] Akansu SO, Dulger Z, Kahraman N, Veziroğlu TN. Internal combustion engines fueled by natural gas-hydrogen mixtures. Int J Hydrogen Energy 2004; 29: 1527-39.

[15] Akansu SO, Kahraman N, Çeper B. Experimental study on a spark ignition engine fuelled by methane-hydrogen mixtures. Int J Hydrogen Energy 2007; 32: 4279-84.

[16] Kahraman N, Çeper B, Akansu SO, Aydin K. Investigation of combustion characteristics and emissions in a spark-ignition engine fuelled with natural gas-hydrogen blends. Int J Hydrogen Energy 2009; 34: 1026-34.

[17] Akansu SO, Bayrak M. Experimental study of a spark ignition engine fueled by $CH_4/H_2$ (70/30) and LPG. Int J Hydrogen Energy 2011; 36: 9260-6.

[18] Mariani A, Morrone B, Unich A. Numerical evaluation of internal combustion spark ignition engines performance fuelled with hydrogen – Natural gas blends. Int J Hydrogen Energy 2012; 37: 2644-54.

[19] Klell M, Eichlseder H, Sartory M. Mixtures of hydrogen and methane in the internal combustion engine - Synergies, potential and regulations. Int J Hydrogen Energy 2012; 37: 11531-40.

[20] Acikgoz B, Celik C. An experimental study on performance and emission characteristics of a methane-hydrogen fuelled gasoline engine. Int J Hydrogen Energy 2012; 37: 18492-7.

[21] Navarro E, Leo TJ, Corral R. $CO_2$ emissions from a spark ignition engine operating on natural gas–hydrogen blends (HCNG). Appl Energy 2013; 101: 112-20.

[22] Thurnheer T, Soltic P, Eggenschwiller PD. S.I. engine fuelled with gasoline, methane and methane/hydrogen blends: Heat release and loss analysis. Int J Hydrogen Energy 2009; 34: 2494-503.

[23] Ceper BA, Akansu SO, Kahraman N. Investigation of cylinder pressure for $H_2/CH_4$ mixtures at different loads. Int J Hydrogen Energy 2009; 34: 4855-4861.

[24] Ma F, Wang Y, Ding S, Jiang L. Twenty percent hydrogen-enriched natural gas transient performance research. Int J Hydrogen Energy 2009; 34: 6523-31.

[25] Xu J, Zhang X, Liu J, Fan L. Experimental study of a single-cylinder engine fuelled with natural gas-hydrogen mixtures. Int J Hydrogen Energy 2010; 35: 2909-14.

[26] Porpatham E, Ramesh A, Nagalingam B. Effect of hydrogen addition on the performance of a biogas fuelled spark ignition engine. Int J Hydrogen Energy 2007; 32: 2057-65.

[27] Porpatham E, Ramesh A, Nagalingam B. Investigation on the effect of concentration of methane in biogas when used as a fuel for a spark ignition engine. Fuel 2008; 87: 1651-9.

[28] Jeong C, Kim T, Lee K, Song S, Chun KM. Generating efficiency and emissions of a spark-ignition gas engine generator fuelled with biogas-hydrogen blends. Int J Hydrogen Energy 2009; 34: 9620-7.

[29] Lee K, Kim T, Cha H, Song S, Chun KM. Generating efficiency and $NO_x$ emissions of a gas engine generator fuelled with a biogas-hydrogen blend and using an exhaust gas recirculation system. Int J Hydrogen Energy 2010; 35: 5723-30.

[30] Arroyo J, Moreno F, Muñoz M, Monné C. Efficiency and emissions of a spark ignition engine fueled with synthetic gases obtained from catalytic decomposition of biogas. Int J Hydrogen Energy 2013; 38: 3784-92.

[31] Laget O, Richard S, Serrano D, Soleri D. Combining experimental and numerical investigations to explore the potential of downsized engines operating with methane/hydrogen blends. Int J Hydrogen Energy 2012; 37: 11514-30.

[32] Ma F, Wang Y, Liu H, Li Y, Wang J, Zhao S. Experimental study on thermal efficiency and emission characteristics of a lean burn hydrogen enriched natural gas engine. Int J Hydrogen Energy 2007; 32: 5067-75.

[33] Wang Y, Zhang X, Li C, Wu J. Experimental and modeling study of performance and emissions of SI engine fuelled by natural gas-hydrogen mixtures. Int J Hydrogen Energy 2010; 35: 2680-3.

[34] Park C, Kim C, Choi Y. Power output characteristics of hydrogen-natural gas blend fuel engine at different compression ratios. Int J Hydrogen Energy 2012; 37: 8681-7.

[35] Wang J, Chen H, Liu B, Huang Z. Study of cycle-by-cycle variations of a spark ignition engine fueled with natural gas-hydrogen blends. Int J Hydrogen Energy 2008; 33: 4876-83.

[36] Genovese A, Contrisciani N, Ortenzi F, Cazzola V. On road experimental tests of hydrogen/natural gas blends on transit buses. Int J Hydrogen Energy 2011; 36: 1775-83.

[37] Park C, Kim C, Choi Y, Sangyeon, Won S, Moriyoshi Y. The influences of hydrogen on the performance and emission characteristics of a heavy duty natural gas engine. Int J Hydrogen Energy 2011; 36: 3739-45.

[38] Sopena C, Diéguez PM, Sáinz D, Urroz JC, Guelbenzu E, Gandía LM. Conversion of a commercial spark ignition engine to run on hydrogen: Performance comparison using hydrogen and gasoline. Int J Hydrogen Energy 2010; 35: 1420-9.

[39] Sáinz D, Diéguez PM, Urroz JC, Sopena C, Guelbenzu E, Pérez-Ezcurdia A, Benito-Amurrio M, Marcelino-Sádaba S, Arzamendi G, Gandía LM. Conversion of a gasoline engine-generator set to a bi-fuel (hydrogen/gasoline) electronic fuel-injected power unit. Int J Hydrogen Energy 2011; 36: 13781-92.

[40] Sáinz D, Diéguez PM, Sopena C, Urroz JC, Gandía LM. Conversion of a commercial gasoline vehicle to run bi-fuel (hydrogen-gasoline). Int J Hydrogen Energy 2012; 37: 1781-9.

[41] Gandía LM, Oroz, R, Ursúa A, Sanchis P, Diéguez PM. Renewable Hydrogen Production: Performance of an Alkaline Water Electrolyzer Working under Emulated Wind Conditions. Energy & Fuels 2007; 21: 1699-706.

[42] Diéguez PM, Ursúa A, Sanchis P, Sopena C, Guelbenzu E, Gandía LM. Thermal performance of a commercial alkaline water electrolyzer: Experimental study and mathematical modeling. Int J Hydrogen Energy 2008; 33: 7338-54.

[43] Ursúa A, Marroyo L, Gubía E, Gandía LM, Diéguez PM, Sanchis P. Influence of the power supply on the energy efficiency of an alkaline water electrolyser. Int J Hydrogen Energy 2009; 34: 3221-33.

[44] Ursúa A, Gandía LM, Sanchis P. Hydrogen production from water electrolysis: current status and future trends. Proc IEEE 2012; 100: 410-26.

[45] Moreno F, Muñoz M, Arroyo J, Magén O, Monné C, Suelves I. Efficiency and emissions in a vehicle spark ignition engine fueled with hydrogen and methane blends. Int J Hydrogen Energy 2012; 37: 11495-503.

[46] Moran MJ, Shapiro HN. Fundamentals of Engineering Thermodynamics. 5th ed. Chichester: John Wiley & Sons; 2006.

[47] Knop V, Benkenida A, Jay S, Colin O. Modelling of combustion and nitrogen oxide formation in hydrogen-fuelled internal combustion engines within a 3D CFD code. Int J Hydrogen Energy 2008; 33: 5083-97.

[48] Moreno F, Arroyo FJ, Muñoz M, Monné C. Combustion analysis of a spark ignition engine fueled with gaseous blends containing hydrogen. Int J Hydrogen Energy 2012; 37: 13564-73.

[49] Tinaut FV, Melgar A, Giménez B, Reyes M. Prediction of performance and emissions of an engine fuelled with natural gas/hydrogen blends. Int J Hydrogen Energy 2011; 36: 947-56.

[50] Wang X, Zhang H, Yao B, Lei Y, Sun X, Wang D, Ge Y. Experimental study on factors affecting lean combustion limit of S.I engine fueled with compressed natural gas and hydrogen blends. Energy 2012; 38: 58-65.

[51] Park J, Cha H, Song S, Chun KM. A numerical study of a methane-fueled gas engine generator with addition of hydrogen using cycle simulation and DOE method. Int J Hydrogen Energy 2011; 36: 5153-62.

## Captions

Table 1. Influence of the spark advance on the peak pressure and $NO_x$ concentration in the exhaust for engine operation on pure hydrogen at $\lambda$ = 1.6 and 2000 rpm.

Fig. 1. Evolution of the adiabatic flame temperature as a function of the air-to-fuel ratio ($\lambda$) and the methane molar fraction ($\eta$) of the fuel.

Fig. 2. Evolution of the engine brake torque as a function of $\lambda$ and the fuel composition at full load, 3400 rpm and optimum spark advance.

Fig. 3. Evolution of the thermal efficiency as a function of $\lambda$ and the fuel composition at full load, 4200 rpm and optimum spark advance.

Fig. 4. Pressure-volume diagrams corresponding to the thermodynamic cycles developed under the operating conditions of Table 1.

Fig. 5. Heat release rate diagram corresponding to the thermodynamic cycle developed under the operating conditions included in Table 1 at spark advance of 10 º BTDC.

Fig. 6. Evolution of the specific $NO_x$ emissions as a function of the spark advance and fuel composition at full load, $\lambda$ = 1.6 and 3400 rpm.

Fig. 7. Evolution of the specific $NO_x$ emissions as a function of $\lambda$ and fuel composition at full load, 2000 rpm and optimum spark advance.

Fig. 8. Evolution of the specific CO emissions as a function of the spark advance and fuel composition at full load and $\lambda$ = 1.6. Solid and dash-dotted lines correspond to engine speeds of 4200 and 3400 rpm, respectively.

Fig. 9. Evolution of the specific CO emissions as a function of $\lambda$ and fuel composition at full load, 3400 rpm and optimum spark advance.

Fig. 10. Evolution of the specific unburned hydrocarbons emissions as a function of the spark advance and fuel composition at full load and $\lambda$ = 1.6. Solid, dotted, dash-dotted and dashed lines correspond to engine speeds of 4200, 3400, 2600 and 1800 rpm, respectively.

Fig. 11. Evolution of the specific unburned hydrocarbons emissions as a function of $\lambda$ and fuel composition at full load and optimum spark advance. Solid, dotted, dash-dotted and dashed lines correspond to engine speeds of 4200, 3400, 2600 and 1800 rpm, respectively.

Table 1.

| Spark advance (º BTDC) | $\dot{V}_f$ (Nl/min) | Brake power (kW) | Maximum pressure (bar) | $C_{NO_x}$ (ppm) |
|---|---|---|---|---|
| 10 | 155.4 | 10.6 | 40.7 | 113 |
| 15 | 155.4 | 10.7 | 46.0 | 159 |
| 20 | 155.6 | 10.6 | 50.1 | 214 |

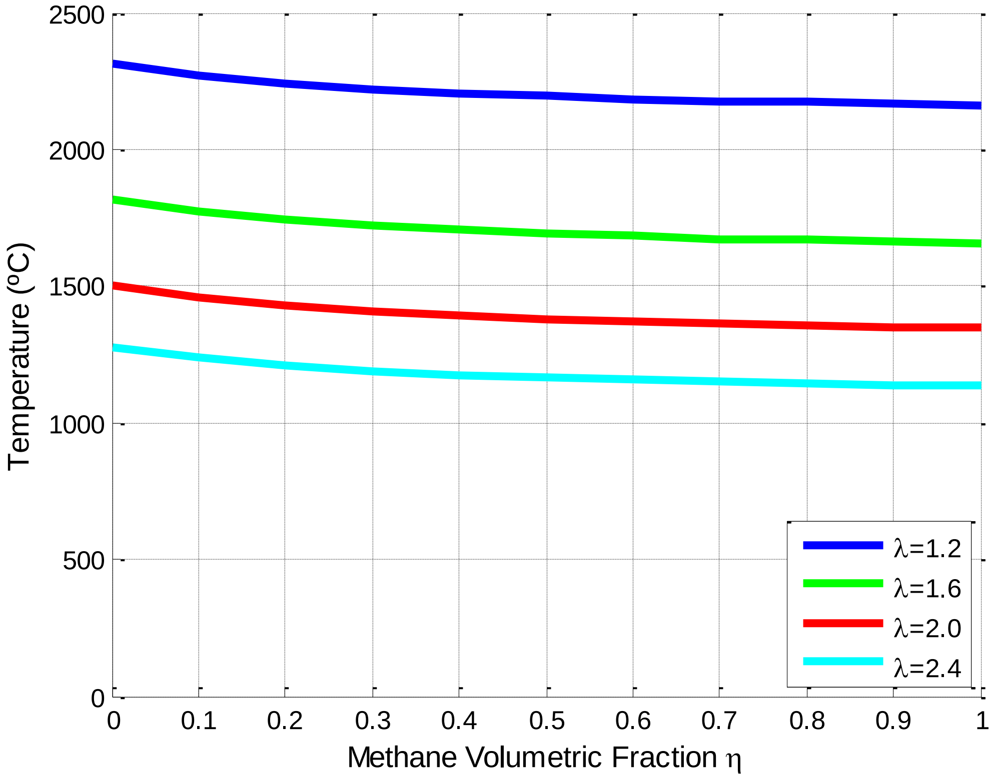

2500
2000
1500
1000
500
0
0
0.1
0.2
0.3
0.4
0.5
0.6
0.7
0.8
0.9
1
Temperature (ºC)
Methane Volumetric Fraction η
λ=1.2
λ=1.6
λ=2.0
λ=2.4


**Fig. 1.**

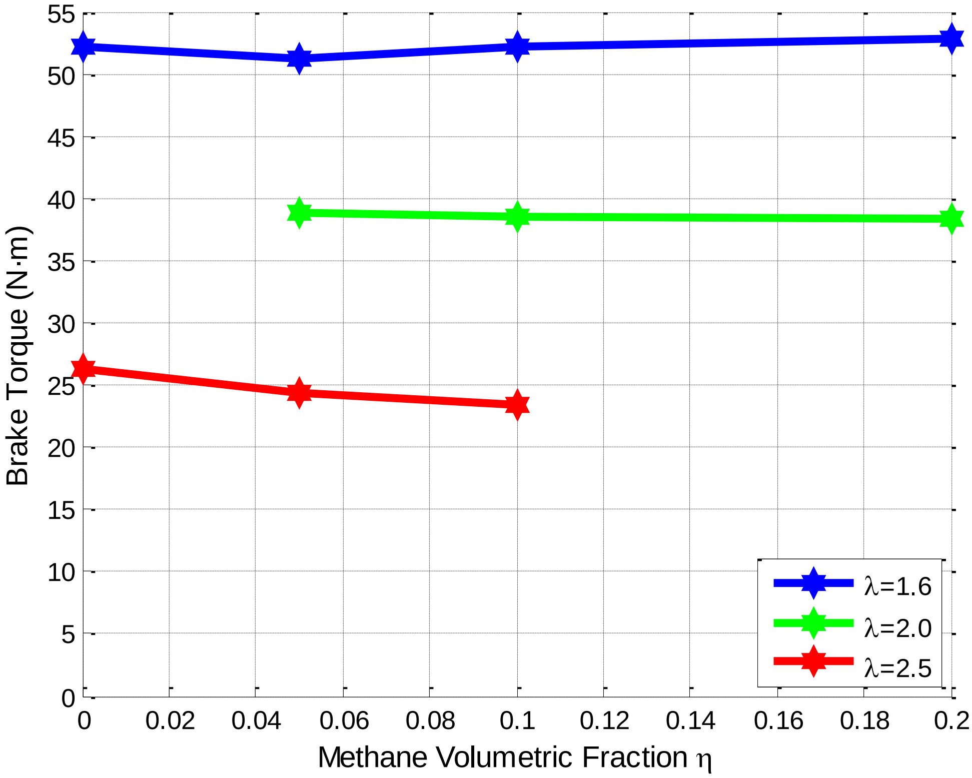

Brake Torque (N·m)
Methane Volumetric Fraction η
λ=1.6
λ=2.0
λ=2.5
0
5
10
15
20
25
30
35
40
45
50
55
0
0.02
0.04
0.06
0.08
0.1
0.12
0.14
0.16
0.18
0.2


**Fig. 2.**

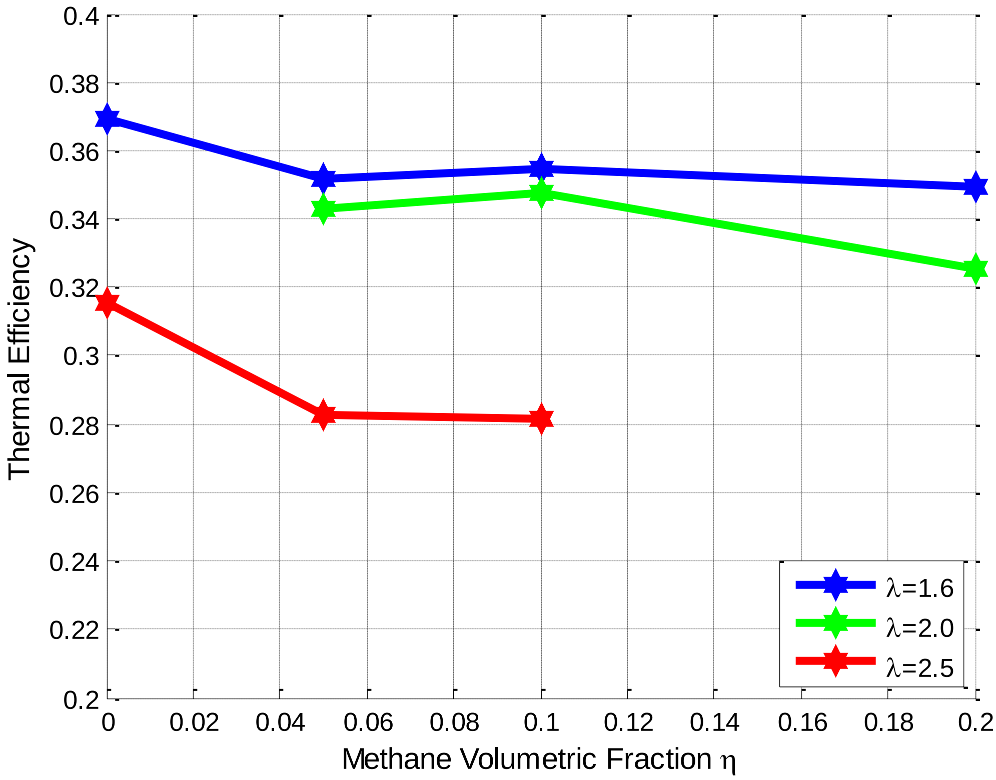
Thermal Efficiency
0.4
0.38
0.36
0.34
0.32
0.3
0.28
0.26
0.24
0.22
0.2
0
0.02
0.04
0.06
0.08
0.1
0.12
0.14
0.16
0.18
0.2
Methane Volumetric Fraction η
λ=1.6
λ=2.0
λ=2.5

**Fig. 3.**

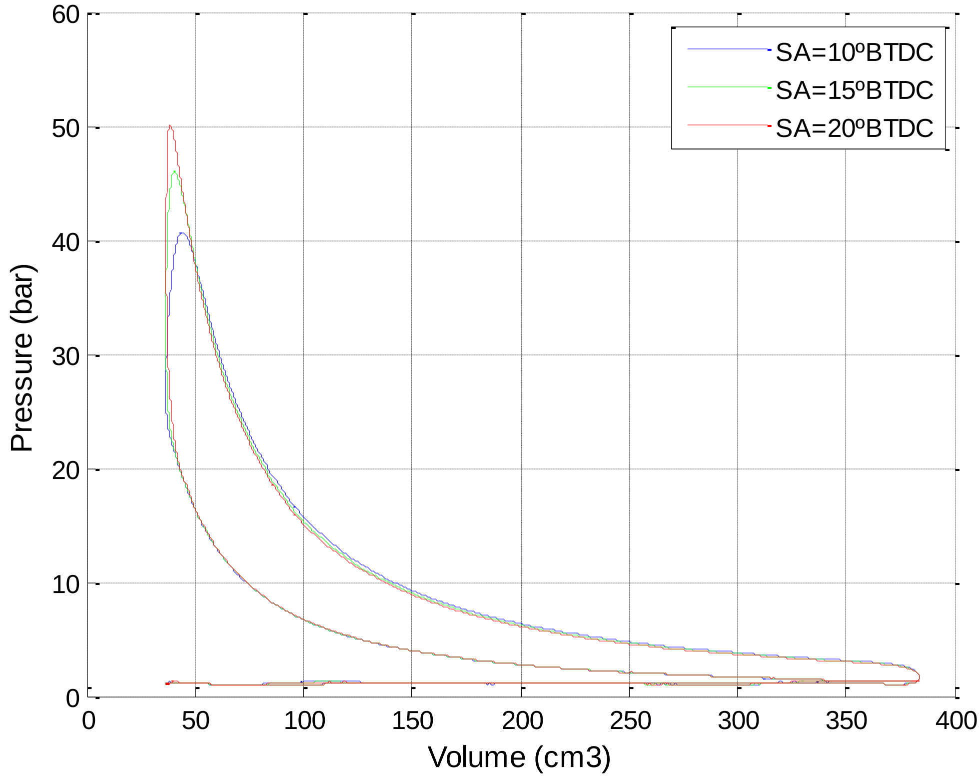
SA=10ºBTDC
SA=15ºBTDC
SA=20ºBTDC
Pressure (bar)
Volume (cm3)
0
10
20
30
40
50
60
0
50
100
150
200
250
300
350
400

**Fig. 4.**

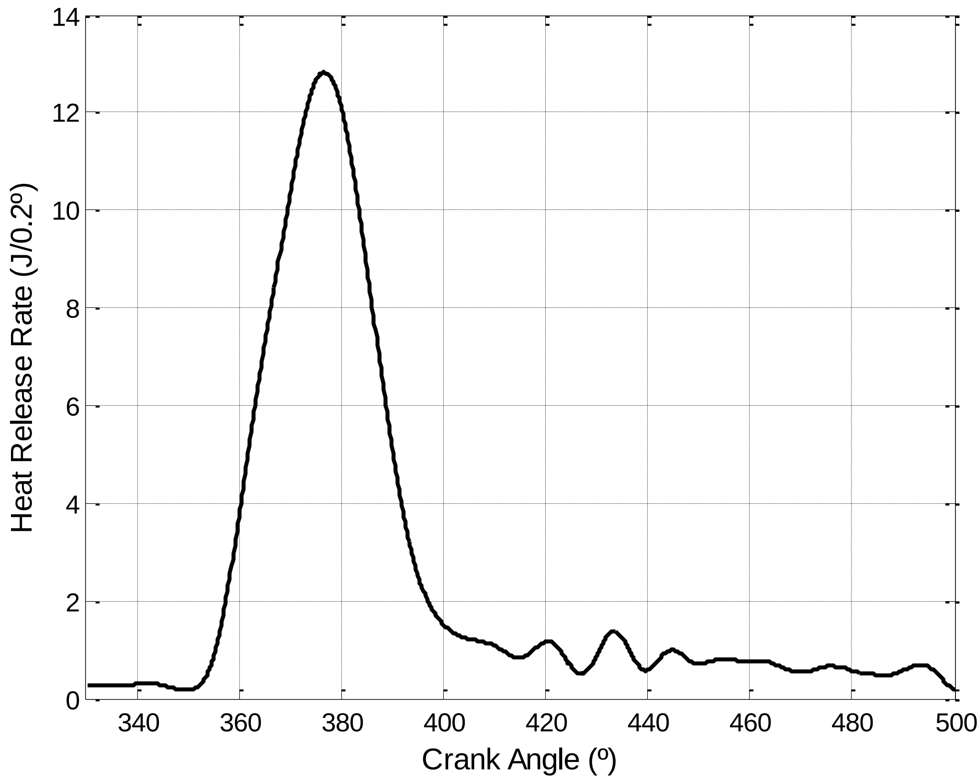
Heat Release Rate (J/0.2º)
0
2
4
6
8
10
12
14
340
360
380
400
420
440
460
480
500
Crank Angle (º)

**Fig. 5.**

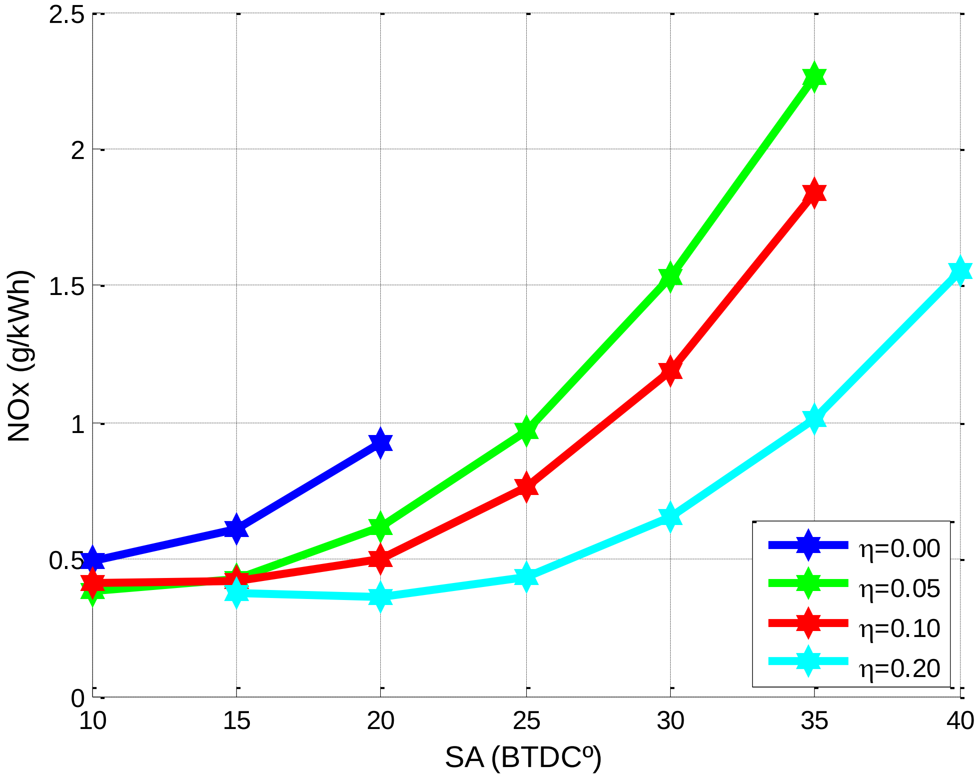

NOx (g/kWh)
SA (BTDCº)
2.5
2
1.5
1
0.5
0
10
15
20
25
30
35
40
η=0.00
η=0.05
η=0.10
η=0.20


**Fig. 6.**

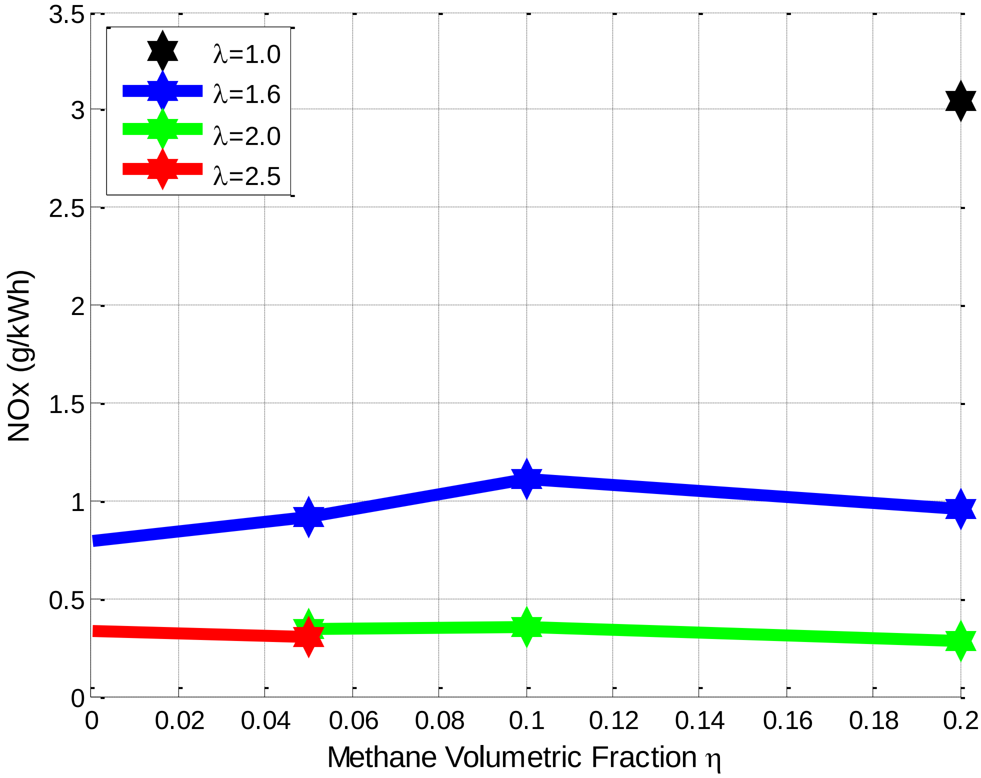
λ=1.0
λ=1.6
λ=2.0
λ=2.5
NOx (g/kWh)
3.5
3
2.5
2
1.5
1
0.5
0
0
0.02
0.04
0.06
0.08
0.1
0.12
0.14
0.16
0.18
0.2
Methane Volumetric Fraction η

**Fig. 7.**

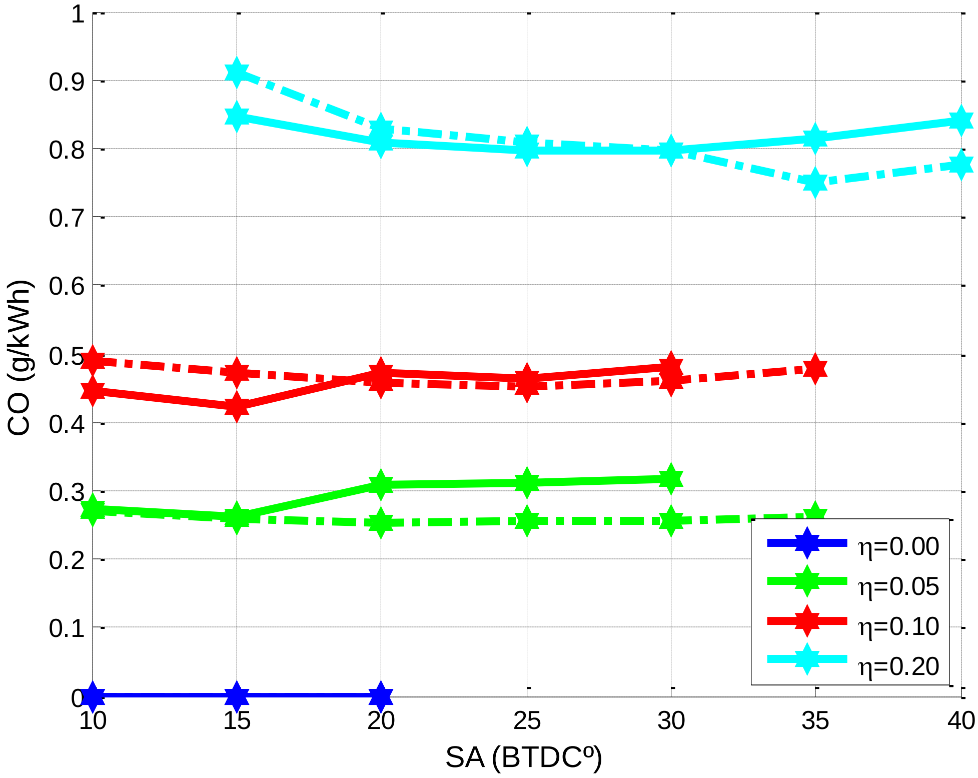

CO (g/kWh)
SA (BTDCº)
0
0.1
0.2
0.3
0.4
0.5
0.6
0.7
0.8
0.9
1
10
15
20
25
30
35
40
η=0.00
η=0.05
η=0.10
η=0.20


**Fig. 8.**

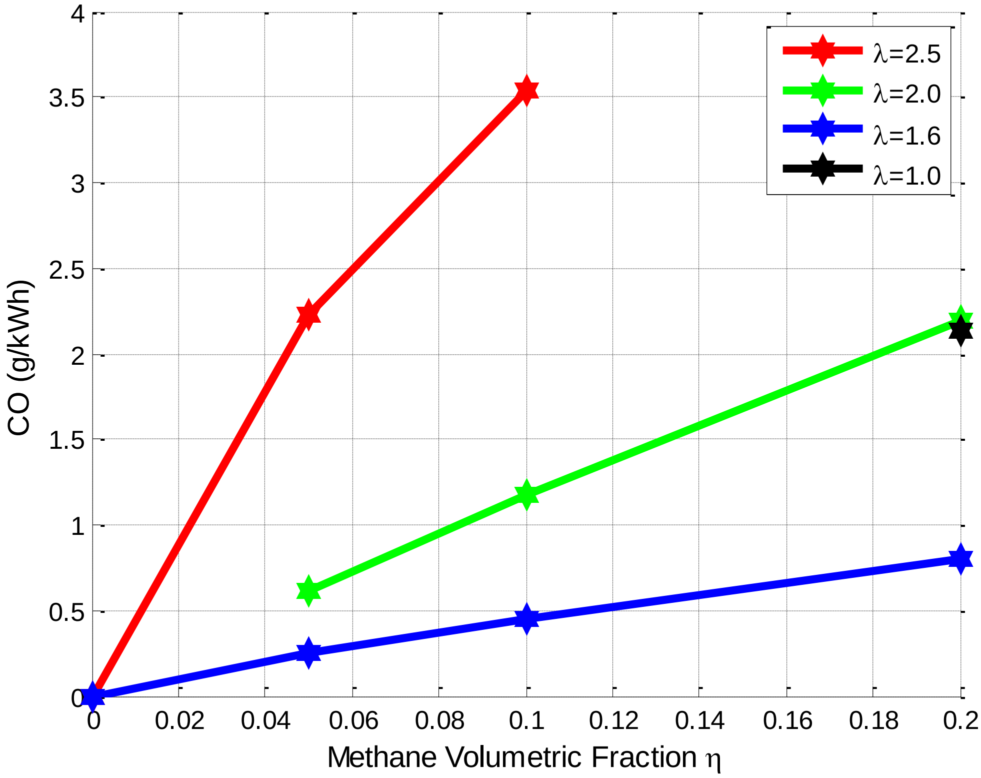
λ=2.5
λ=2.0
λ=1.6
λ=1.0
CO (g/kWh)
Methane Volumetric Fraction η
0
0.5
1
1.5
2
2.5
3
3.5
4
0
0.02
0.04
0.06
0.08
0.1
0.12
0.14
0.16
0.18
0.2

**Fig. 9.**

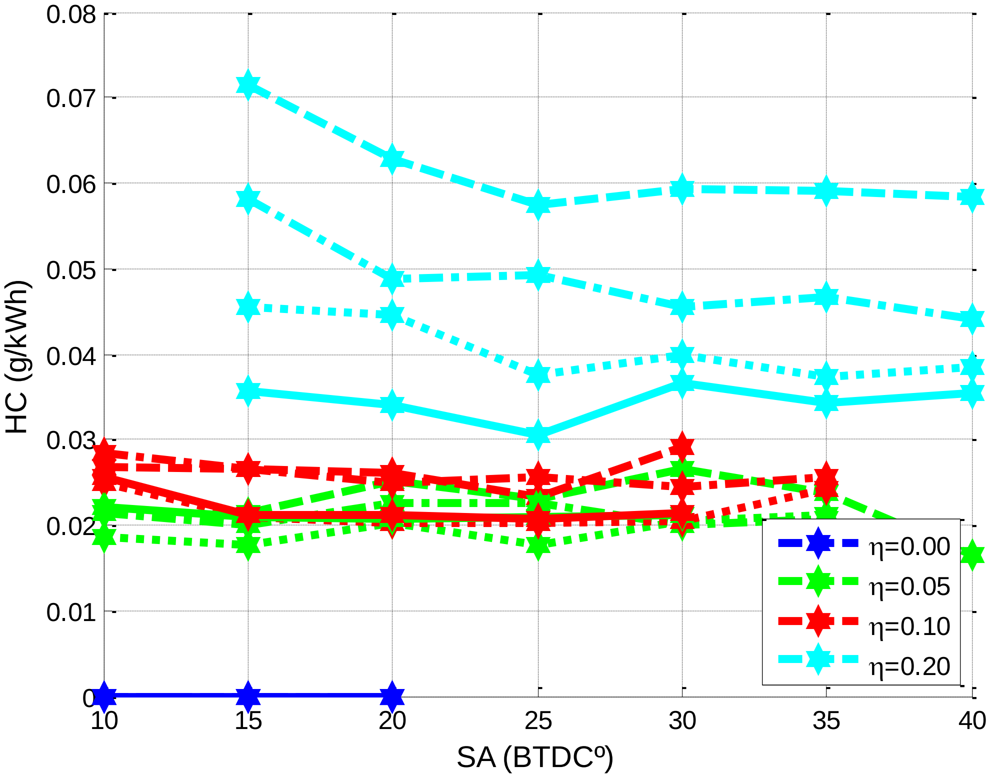
HC (g/kWh)
0.08
0.07
0.06
0.05
0.04
0.03
0.02
0.01
0
10
15
20
25
30
35
40
SA (BTDCº)
η=0.00
η=0.05
η=0.10
η=0.20

**Fig. 10.**

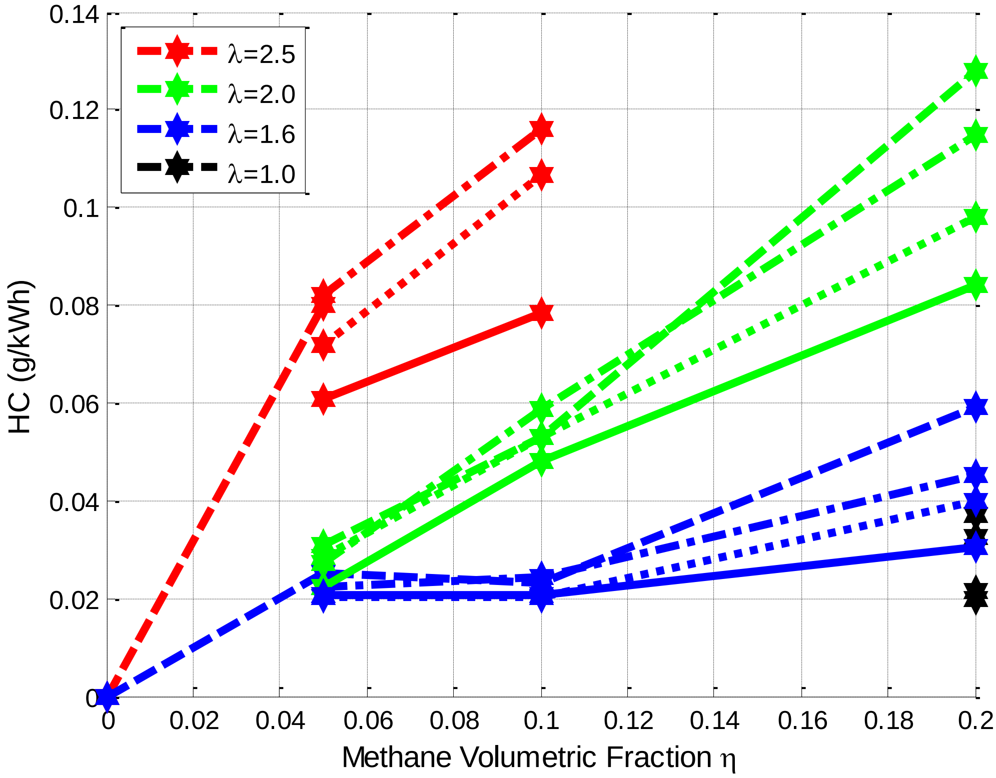
λ=2.5
λ=2.0
λ=1.6
λ=1.0
0.14
0.12
0.1
0.08
0.06
0.04
0.02
0
HC (g/kWh)
0
0.02
0.04
0.06
0.08
0.1
0.12
0.14
0.16
0.18
0.2
Methane Volumetric Fraction η

**Fig. 11.**